



Article

Discovering Novel Glass with Robust Crystallization Resistance via Amorphous Phase Separation Engineering

Mou Deng ¹, Mingzhong Wang ^{1,2}, Yu Rao ¹, Yinsheng Xu ^{3,*}, Dong Wu ¹, Shisheng Lin ⁴ and Ping Lu ^{1,*}

¹ School of Materials Science and Engineering, Wuhan University of Technology, Wuhan 430070, China; 268778@whut.edu.cn (M.D.); wangmz@csholding.com (M.W.); 245800@whut.edu.cn (Y.R.); dongwu@whut.edu.cn (D.W.)

² Yichang CSG Photovoltaic Glass Co., Ltd., Yichang 443000, China

³ State Key Laboratory of Silicate Materials for Architectures, Wuhan University of Technology, Wuhan 430070, China

⁴ College of Physics and Energy, Fujian Normal University, Fuzhou 350117, China; linshisheng@fjnu.edu.cn

* Correspondence: xuyinsheng@whut.edu.cn (Y.X.); lupingwh@whut.edu.cn (P.L.)

Abstract: Amorphous phase separation (APS) is ubiquitously found in a large number of glass systems, because the glass can be regarded as solid with a heterogeneous structure at the nanoscale. However, little attention has been paid to the big challenges in utilizing APS in searching novel amorphous glass from above to below, which highlights the meticulous microstructure tunability of glass. Correspondingly, we develop a novel $\text{SiO}_2\text{-Al}_2\text{O}_3\text{-P}_2\text{O}_5\text{-Li}_2\text{O}\text{-ZrO}_2$ glass with APS (SAPLZ APS) which has robust crystallization resistance via the APS engineering. A comparative study is conducted to reveal the APS–crystallization property relationship. It can be found that the introduced APS can substantially impede the precipitated crystal growth in the studied glass system. Considering detailed glassy structure and microstructure, a diffusion barrier around each Li-rich droplet is created by the presence of P^{5+} concentration surrounding the Li-rich region. Meanwhile, due to the increase in Q^4 at the expense of Q^3 , the polymerization degree in the Si-rich amorphous area can be enhanced, further increasing its viscosity and raising the kinetic barrier of Si-related crystal growth. These findings provide a new manner to develop new glass with superior anti-crystallization performance.



Citation: Deng, M.; Wang, M.; Rao, Y.; Xu, Y.; Wu, D.; Lin, S.; Lu, P.

Discovering Novel Glass with Robust Crystallization Resistance via Amorphous Phase Separation Engineering. *Inorganics* **2024**, *12*, 149. <https://doi.org/10.3390/inorganics12060149>

Academic Editors: Guido Kickelbick and Torben R. Jensen

Received: 17 April 2024

Revised: 11 May 2024

Accepted: 28 May 2024

Published: 29 May 2024



Copyright: © 2024 by the authors. Licensee MDPI, Basel, Switzerland. This article is an open access article distributed under the terms and conditions of the Creative Commons Attribution (CC BY) license (<https://creativecommons.org/licenses/by/4.0/>).

1. Introduction

Glass ceramics, as an attractive and versatile material, are generated via controlled crystallization to precipitate microcrystals/nanocrystals within a glass matrix [1,2]. The properties of GCs are largely determined by the properties and composition of their crystalline phase. Lithium aluminum silicate (LAS) GCs have been widely studied because of their low coefficient of thermal expansion and high mechanical strength and transparency [3–6]. In this regard, the process of glass crystallization involves two distinct stages: nucleation and crystal growth. Amorphous phase separation (APS) plays a significant role in nucleation and has following influences on the subsequent crystal growth.

From the past until now, and even in the future, as the inherent character of glass (perceived as a “super-cooled liquid”) changes, studies on APS have been and will be crucial in the field of glass science [7–12]. In fact, since glass can be regarded as solid with a heterogeneous structure at the nanoscale, APS is ubiquitously found in a large number of glass systems (e.g., fluoroaluminosilicate glass, fluorosilicate glass, halidephosphate glass, and chalcogenide glass). In terms of silicate glass, its APS should be caused by the occurrence of competition between different cations for oxygen ions; whereas the bridging oxygen ions are arranged around silicon ions in the form of silicon–oxygen tetrahedra, the non-bridging oxygen ions are pulled by network modifiers or intermediate ions to satisfy their respective structural arrangements [13]. When P_2O_5 is added to the glass, it tends to

phase separate the glass and form enriched domains with distinct glassy components by removing non-bridging, oxygen-forming lithium ions from the silicate network [14].

Prof. Zanotto measured the nucleation kinetics of the barium disilicate crystal phase in BaO-SiO₂ glass utilizing a quantitative optical microscope in the temperature range of 673–807 °C in 1986 [15]. It was found that the nucleation rate of amorphous phase separation glass is much lower than that of 33.1% mol% BaO glass, which is close to the composition without phase separation. However, the effect of phase separation on crystallization nucleation is substantial but indirect, due to changes in the composition of the barium-rich phase that undergoes crystallization nucleation. Therefore, after 1 h of heat treatment at low temperatures, the separation of amorphous phases can be ignored. The higher the BaO content in the glass, the higher the nucleation rate of the crystals, which is closer to the stoichiometric composition of disilicates. After heat treatment at higher temperatures where phase separation occurs, the nucleation rate of crystals in phase-separated glass tends to converge due to the very similar matrix composition in the glass at a given temperature. Prof. Zanotto released a significant paper in 2020 [16], which reviewed the most applicable results of a research project on the synchronous crystallization kinetics analysis of APS, BaO-SiO₂, and Li₂O-SiO₂ glass, and supplemented recent research findings. The authors consider the following: First, the influence of the droplet interface can be neglected, as they are two orders of magnitude smaller compared to the crystal/nucleus surface energy. Second, the crystal nucleation kinetics of the phase-separating glasses exhibit an initial increase and subsequently reach a constant value as the composition of the liquid matrix attains the binodal boundary. Finally, the APS behavior drives the composition of the glass matrix towards the stoichiometric composition of the barium disilicate crystal phase, thereby enhancing the crystal nucleation rate, but it never reaches the value of the stoichiometric composition of the barium disilicate crystal glass. These comprehensive results clearly indicate that the primary function of APS is to transform the composition of the glass matrix into a stoichiometric crystal phase composition, thereby leading to enhanced crystal nucleation. These discoveries have solved a long-standing mystery in glass science.

Prof. Zanotto demonstrated the ubiquity of this phenomenon, showing the possible effect of APS. There are generally two significant impacts of APS: promoting nucleation and forming self-organization [17]. The former shifts the composition of the separating glass towards that of the stoichiometric crystal phase, where APS acts as a special catalyst for nucleation [18]. The latter forms the diffusion barrier around each APS droplet, inhibiting crystal growth tendency [19]. As such, when precursor glass is subjected to phase separation treatment, a discernible reduction in the size of crystalline grains will be observed, which is beneficial to controlling crystallization and obtaining nanometer-sized crystals in glass [20]. Great endeavors have been undertaken to reveal APS [21–23]. Despite their successes, little attention has been paid to the big challenges in utilizing APS engineering in searching novel amorphous glass from above to below, which highlights the meticulous microstructure tunability of glass.

Herein, we develop a new amorphous glass with robust crystallization resistance, the SiO₂-Al₂O₃-P₂O₅-Li₂O-ZrO₂ glass with APS (abbreviated as SAPLZ APS), via *in situ* APS of the glass matrix. A comprehensive study was conducted to unearth the APS type, glassy structure, microstructure, and crystallization performance in the studied glass system. The controlled APS progress leads to the highly ordered, Li-rich glassy particles (surrounded by P⁵⁺) and Si-rich glassy components in the glass network, forming a diffusion barrier around each Li-rich droplet and facilitating an enhanced polymerization degree in the Si-rich amorphous area, thus achieving the ingenious control of glassy structure.

2. Experiment

2.1. Synthesis

The precursor glass (PG) with the nominal composition (in mol.%) of 75.34SiO₂-8.00Al₂O₃-1.00P₂O₅-15.67Li₂O-2.0ZrO₂ (abbreviated as SAPLZ glass) was prepared via

the conventional melt-quenching route. A trace of P_2O_5 was used as a nucleation agent to induce phase separation. The preparation process of the precursor glass was as follows. First, we calculated the amount of each oxide required based on the chemical formula of the target crystal. Secondly, we considered which raw materials to utilize to introduce the required oxides. Finally, we calculated the required mass of raw material. This experiment utilized high-quality analytical grade reagents such as SiO_2 ($\geq 99.98\%$), Al_2O_3 ($\geq 99.8\%$), $NH_4H_2PO_4$ ($\geq 99.0\%$), Li_2CO_3 ($\geq 99.9\%$), and ZrO_2 ($\geq 99.8\%$) as raw materials. Weigh the reagents with an electronic balance, placing a new weighing paper on the balance to protect it, and perform a tare operation before each weighing. When weighing, it is advisable to add reagents in small amounts and multiple times. Excess samples should not be placed back into the original kit. The operation should be conducted in a stable environment. The errors of the sample should be controlled below 2 mg. Then, transfer the sample to an agate mortar for mixing and grinding for 15 min. During this process, it is necessary to ensure that the sample is initially mixed evenly and the particle size of the reagents is controlled within the same range. Afterwards, use a dry ball mill to stir the raw materials for 1 h. When removing the sample, it is necessary to use dust-free paper to collect as many residual reagents as possible from the machine. After mixing evenly, gradually transfer the mixture to a Pt-Rh (90/10 wt%) crucible. During the transfer process, there are two aspects to be aware of. First, do not shake or vibrate the crucible to avoid the raw materials becoming too compact in the crucible. If the raw materials are too compact when transferred to a high-temperature furnace, it may cause the raw materials to erupt and potentially change the composition. Second, the raw materials should be added to the crucible up to two-thirds of its volume, and if there are too many volatile components in the raw materials, it is best not to exceed one-half of the volume. The melting process of the sample was as follows: we melted the first batch of raw materials added to the crucible at 1500 °C for 10 min, and then removed the crucible and added the remaining raw materials. We repeated the above operation until all the raw materials were added. After preliminary melting at 1500 °C, we heated up to 1620 °C and melted for 1 h under an atmospheric environment. The molten glass was then quickly poured onto a copper plate and rapidly quenched. Another copper plate was used to quickly press the glass. If the glass naturally fractured, the fragments were directly collected and transferred to the crucible. If the glass remained intact, it was crushed, and the glass fragments and powder were completely collected and transferred to the crucible. This step helped to ensure that the glass liquid discharged bubbles and melted evenly. The glass was then placed in a high-temperature furnace and melted at 1620 °C for 2 h under an atmospheric environment. At the end of the operation, the glass melt was poured into a copper mold and pressed between two copper plates. Subsequently, the obtained bulk glasses were cut into square coupons and polished for the following heat treatment. In the first step, the glasses were subjected to phase separation at 600 °C/620 °C/640 °C for different periods of time to produce the APS. In the second step, the samples were further heat-treated at 750 °C, 775 °C, 800 °C for 1, 2, or 4 h to research their crystallization ability. Meanwhile, the as-quenched glass specimens were also heat-treated at 700 °C, 725 °C, 750 °C, 775 °C, 800 °C, and 825 °C for 1 h as reference. The heat treatment procedure for the samples was as follows: the muffle furnace was inspected to ensure it was clean and free of any other samples. The samples were placed in a ceramic boat and positioned at the center of the muffle furnace to ensure uniform heating. The heating program was set with a ramp rate of 10 °C/min. After holding at the target temperature for a sufficient duration, the samples were allowed to cool down to room temperature within the furnace. All heat treatments in this experiment were conducted using the same equipment to avoid temperature variations from different devices. Prior to the experiments, the muffle furnace temperature was set to 600 °C and 700 °C, and the actual temperatures were measured using a thermocouple. The results showed that the actual temperatures were close to the set values, allowing us to rule out any interference from the equipment with the experimental results.

2.2. Characterization

Differential scanning calorimetry (DSC) data of the samples were collected using a Simultaneous Thermal Analyzer (STA 449 F1, NETZSCH, Selb, Germany) in the temperature range of 40–900 °C with a heating rate of 10 °C/min under a constant flow of nitrogen gas. The glass transition temperature T_g and crystallization temperature T_p were measured from the DSC curves. The sample preparation for DSC was as follows: first, the sample was cleaned with ultrasonic deionized water for 5 min, then dried for 20 min, and finally ground into a powder with a particle size of 10–80 microns using an agate mortar. The crucible used in the DSC curve test was a platinum crucible. The phases identified in the samples were observed by X-ray diffraction (XRD, PANalytical X'Pert Pro, Almelo, The Netherlands) using a Cu K α radiation source at 40 kV and 40 mA and scanning from 5° to 80° at the scanning speed of 10°/min. The samples for XRD testing were prepared using a standardized method. First, the samples were crushed in a mold, then transferred to an agate mortar and ground for ten minutes to ensure that the samples were dry and had a particle size of 10–80 μ m. Field emission SEM (Hitachi S-4800, 5 kV, Ibaraki, Japan) was used to observe the crystal morphology and size after crystallization. The SEM sample preparation process was as follows: The sample was placed in mold and crushed. Small glass pieces with smooth and flat surfaces and appropriate dimensions were selected. The fracture surface of the glass was etched with 2 vol% aqueous hydrofluoric acid (HF) for 30 s, cleaned by ultrasonication deionized water for 5 min, and then dried for 20 min (as water on the surface of the sample would seriously affect the test results and the pictures taken would have many stripes). Finally, the glass sputter coated with around 4 nm thick platinum to avoid the charging effect during the SEM analysis. The heat-treated glass samples were characterized using a JEM-1400Plus field emission transmission electron microscope (TEM). Additionally, the corresponding selected area diffraction (SAED) was performed to determine whether crystals had precipitated. The specimens for TEM and SAED analysis were prepared by bombarding the sample with argon gas as accelerating ions to sputter the surface atoms using a multifunctional beam ion dilution device (Gatan PIPS 695, Pleasanton, CA, USA). The thickness of the specimen is 30–40 nm. ^{29}Si and ^{31}P MAS NMR spectra were obtained using 4 mm probes on Bruker AVANCE spectrometers operating at a frequency of 500 MHz. The sample preparation for NMR was the same as that for XRD, and it was possible to directly use the samples prepared for XRD testing. Both XRD and NMR are non-destructive tests, so they would not affect the experimental results. ^{29}Si and ^{31}P MAS NMR spectra were obtained using 4 mm probes on Bruker AVANCE spectrometers operating at a frequency of 500 MHz. The ^{29}Si MAS NMR experiments utilized a rotation rate of 6.0 kHz with a resonance frequency of 99.4 MHz. The pulse length for the 90° excitation was set to 6 μ s, and a cyclic delay of 300 s was utilized. As for ^{31}P MAS NMR, a rotation rate of 12.0 kHz and a resonance frequency of 202.5 MHz were applied. The 90° pulse length was set to 2.8 μ s for quenched samples and 2.9 μ s for heat-treated samples. The cycle delay was adjusted to 80 s for quenched samples and 160 s for heat-treated samples.

3. Results and Discussion

The samples were fabricated via a melt-quenching–thermal annealing route which is easily scalable for mass industrial production. XRD analyses on samples with various heat treatment times at 620 °C all show the amorphous hump coming from the glassy structure (Figure 1a). Transmission electron microscopy (TEM) discloses that the spherical particles of size of 5–9 nm are homogeneously distributed among the glass matrix (Figure 1b). The corresponding selected area electron diffraction (SAED) shows a halo ring (a characteristic of an amorphous phase structure), verifying the occurrence of APS. The ^{31}P magic angle spinning nuclear magnetic resonance (MAS-NMR) spectroscopy reveals huge transformation of the local environment surrounding P before/after being heat-treated at 620 °C and illustrates a broad resonance peak which can be well deconvoluted into three sub-bands (originated from Q 1_2 , Q 1_1 , and Q 0 species, respectively) [24,25], as presented in Figures 1c and 2 and Table 1.

Q^n_m is the structural unit of $[PO_4]$ (n represents the number of P atoms connected to each $[PO_4]$; m represents the number of Al atoms attached to each $[PO_4]$, and $m + n \leq 4$). With the annealing time prolonged from 0.5 h to 4 h, Q^0 and Q^1_1 species with lots of non-bridging oxygens gradually dominate, which gives evidence of the formation of relative isolated $[PO_4]$ -composed groups surrounding Li-rich liquid–liquid immiscibility [26]. Differential scanning calorimeter (DSC) analysis on PG indicates a relatively minor exothermic peak at 645 °C, followed by three distinct and prominent exothermic peaks observed at temperatures of 704 °C, 750 °C, and 825 °C, respectively, while the exothermic peak at 645 °C should be assigned to the APS, since it nearly disappears upon preheating at 620 °C (Figure 1d). Based on more careful observations, with the periods of heat treatment time for APS prolonged, the exothermic peaks (at 704 °C, 750 °C, and 825 °C) slightly shift toward a low temperature. Meanwhile, due to the progressive changes in APS, the glass transition temperature (T_g) increases, which indicates an elevated viscosity and improved glass-forming ability [27]. Combined with the amorphous hump from their X-ray diffraction (XRD) patterns (Figure 1a), a conclusion can be drawn that the APS effect indeed exerts influences on the crystallization kinetics in SAPLZ glass.

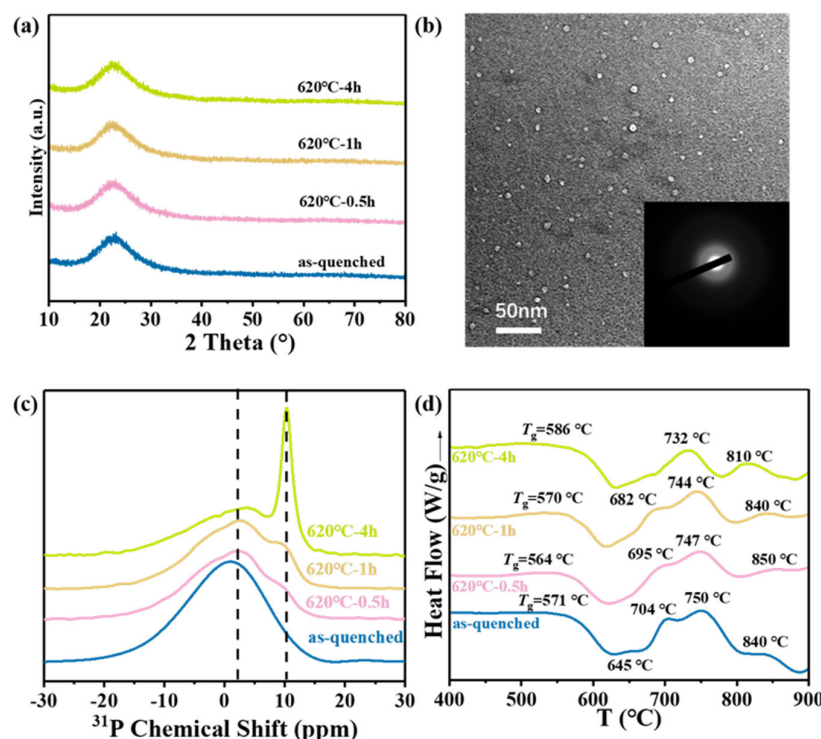


Figure 1. (a) XRD patterns of SAPLZ APS glass. (b) TEM image of SAPLZ APS glass; insets are the corresponding FFT pattern. (c) Solid-state, single-pulse ^{31}P MAS-NMR spectra of SAPLZ glass before/after APS. (d) DSC curve of the SAPLZ glass before/after APS recorded at a heating rate of 10 K/min (T_g denotes the glass transition temperature).

To provide more insights into the local structural transformation in glass before/after APS, ^{29}Si MAS-NMR spectra are exhibited in Figure 3 and Table 2. Obviously, samples exhibit the amorphous nature. Each spectrum can be fitted into three Gaussian peaks, representing the contribution of Q^2 , Q^3 , and Q^4 species (denoted as Q^n , where n represents the number of bridging oxygen atoms for each $[\text{SiO}_4]$) [28,29]. As expected, Q^2 remains relatively stable, Q^3 declines, and Q^4 increases, which indicates the formation of Si-rich glassy components as well as the enhancement of polymerization degree within the glass network, and coincides with the results from the DSC curves (Figure 1d). Based on the discussions above, the valuable insight about the connectivity in the glass structure can

offer crucial information with respect to the type of APS (containing an Li-rich phase surrounded by P^{5+} and a Si-rich phase).

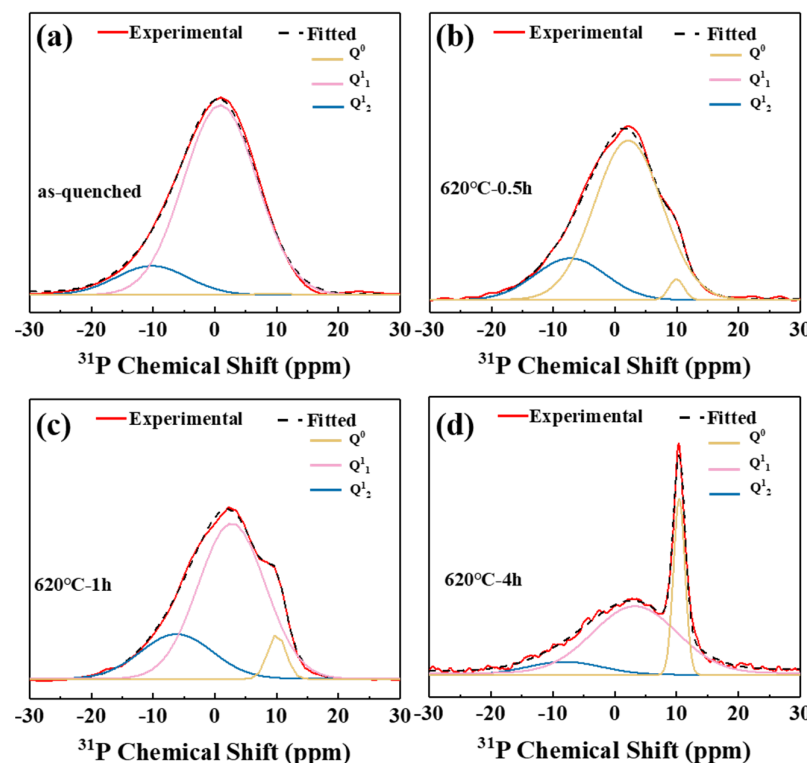


Figure 2. Gaussian fitting of the ^{31}P MAS-NMR spectra of (a) as-quenched PG, (b) $620\text{ }^{\circ}\text{C}-0.5\text{ h}$, (c) $620\text{ }^{\circ}\text{C}-1\text{ h}$, and (d) $620\text{ }^{\circ}\text{C}-4\text{ h}$.

Table 1. The ^{31}P chemical shifts δ_{iso} (± 0.5 ppm) and relative area ($\pm 2\%$) extracted from MAS-NMR spectra.

Sample	As-Quenched PG	$620\text{ }^{\circ}\text{C}-0.5\text{ h}$	$620\text{ }^{\circ}\text{C}-1\text{ h}$	$620\text{ }^{\circ}\text{C}-4\text{ h}$
$Q^0 \delta_{iso}/\text{ppm}$	9.14	9.93	10.01	10.42
$Q^1_1 \delta_{iso}/\text{ppm}$	0.86	2.13	2.62	3.26
$Q^1_2 \delta_{iso}/\text{ppm}$	-10.22	-7.25	-6.6	-8.12
Q^0 Relative area/%	0.34	2.23	5.53	23.59
Q^1_1 Relative area/%	86.70	76.67	73.81	65.29
Q^1_2 Relative area/%	12.96	21.09	20.66	11.13

The SEM observation on SAPLZ glass annealed at $620\text{ }^{\circ}\text{C}$ and $750\text{ }^{\circ}\text{C}$ for different times show their microstructural evolution (Figure 4). It can be seen that the number and size of the precipitated crystal particles show perceivable increases with the annealing duration time at $750\text{ }^{\circ}\text{C}$ prolonged (Figure 4a–c). Fortunately, the crystallinity deviates substantially toward reduction with the APS-producing time increasing from 1 h to 4 h, confirming its inhibitory effect on crystal growth (Figure 4d–i). Specifically, there is a substantial reduction in the number of in situ precipitate crystals in 1 h pre-APS, and only a minimal amount of crystals can be attained after preheating at $620\text{ }^{\circ}\text{C}$ for 4 h. Crystal growth is substantially impeded when the SAPLZ glass undergoes APS, whereby longer APS time leads to a stronger inhibitory effect on crystallization, which provides the evidence for the discovery of a novel amorphous glass with wonderful anti-crystallization performance via the APS process.

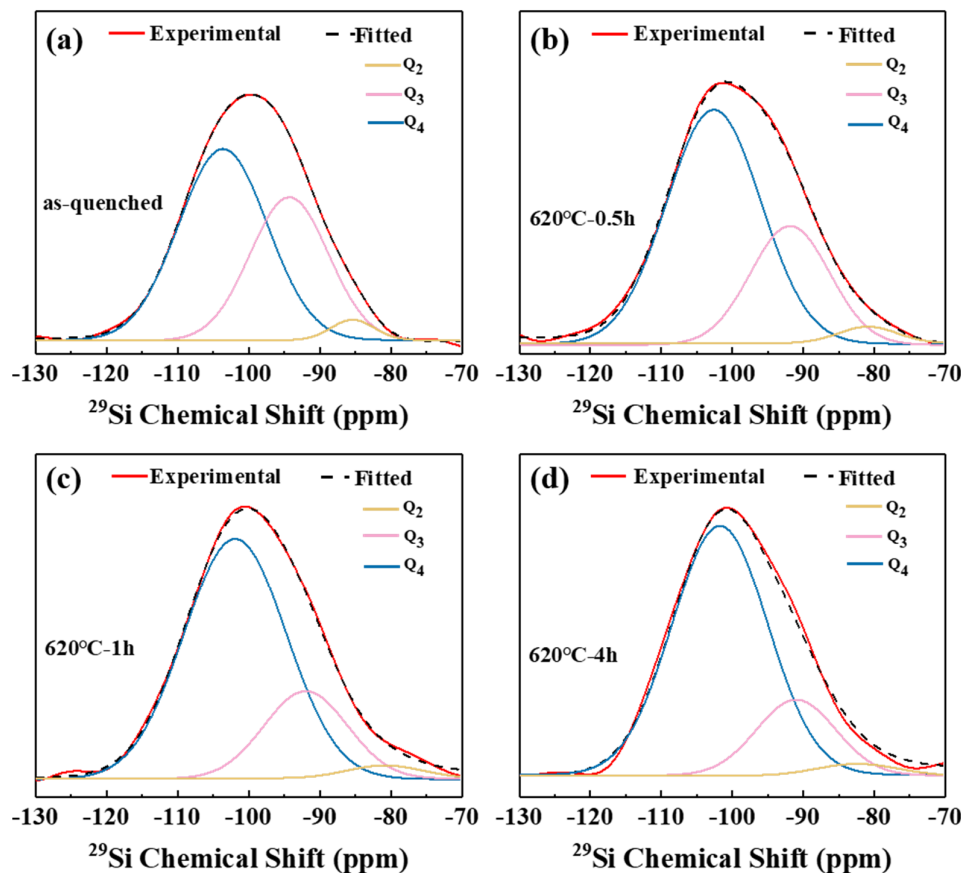


Figure 3. Gaussian fitting of the ^{29}Si MAS-NMR spectra of (a) as-quenched PG, (b) $620\text{ }^{\circ}\text{C}-0.5\text{ h}$, (c) $620\text{ }^{\circ}\text{C}-1\text{ h}$, and (d) $620\text{ }^{\circ}\text{C}-4\text{ h}$.

Table 2. The ^{29}Si chemical shifts δ_{iso} (± 0.5 ppm) and relative area ($\pm 2\%$) extracted from MAS NMR spectra.

Sample	As-Quenched PG	$620\text{ }^{\circ}\text{C}-0.5\text{ h}$	$620\text{ }^{\circ}\text{C}-1\text{ h}$	$620\text{ }^{\circ}\text{C}-4\text{ h}$
$Q^{(2)} \delta_{iso}/\text{ppm}$	-85.38	-80.90	-80.85	-82.37
$Q^{(3)} \delta_{iso}/\text{ppm}$	-94.30	-91.86	-91.98	-91.00
$Q^{(4)} \delta_{iso}/\text{ppm}$	-103.62	-102.60	-101.91	-101.74
$Q^{(2)}$ Relative area/%	3.04	3.01	2.96	3.17
$Q^{(3)}$ Relative area/%	38.71	28.95	22.28	19.45
$Q^{(4)}$ Relative area/%	58.25	68.04	74.76	77.38

To search the novel amorphous glass with strong crystallization resistance, the detailed effect of APS on SAPLZ glass crystallization performances are surveyed. When the heat treatment temperature increases to $725\text{ }^{\circ}\text{C}$, the phase transformation from amorphous to crystalline (tetragonal SiO_2) occurs (Figure 5a), at which point the crystallinity is 2.14%. When the heat treatment temperature further increases from $775\text{ }^{\circ}\text{C}$ to $825\text{ }^{\circ}\text{C}$, the signal of tetragonal $\text{LiAlSi}_2\text{O}_6$ becomes gradually stronger for the samples, and the crystallinity of the sample reaches 74.63%. Fortunately, after introducing the APS process, the adverse crystallization process is effectively restrained (Figure 5b), for instance, at a crystallization temperature of $750\text{ }^{\circ}\text{C}$ and a phase separation temperature of $600\text{ }^{\circ}\text{C}$, the crystallinity was 1.32%. At a phase separation temperature of $640\text{ }^{\circ}\text{C}$, the crystallinity increased to 10.07%. However, at a phase separation temperature of $620\text{ }^{\circ}\text{C}$, no crystal nucleation was observed. The final APS temperature is optimized to $620\text{ }^{\circ}\text{C}$, based on the consideration of its best crystallization resistance behavior. As illustrated in Figure 5c, the SAPLZ APS glass exhibits superior anti-crystallization performance: the heat treatment time is $\sim 4\text{ h}$ at

750 °C to a reach crystallinity of ~45% (in comparison, the heat-treatment time is only ~1 h for SAPLZ glass). When we thermally anneal the samples at 620 °C for different sintering times and then heat-treat them at 750 °C for 1 h, the X-ray diffraction peaks intensity is reduced with the increased APS time, and correspondingly, the crystallinity decreases from 43.7% to 0 via calculating the crystallization fraction (Figure 5d and Table 3), which demonstrates the well-suppressed crystal growth effect from APS for SAPLZ glass. Based on the results above, it can be seen that a kind of novel amorphous material possessing robust crystallization resistance, SAPLZ APS glass (620 °C-4 h), is successfully fabricated via APS engineering.

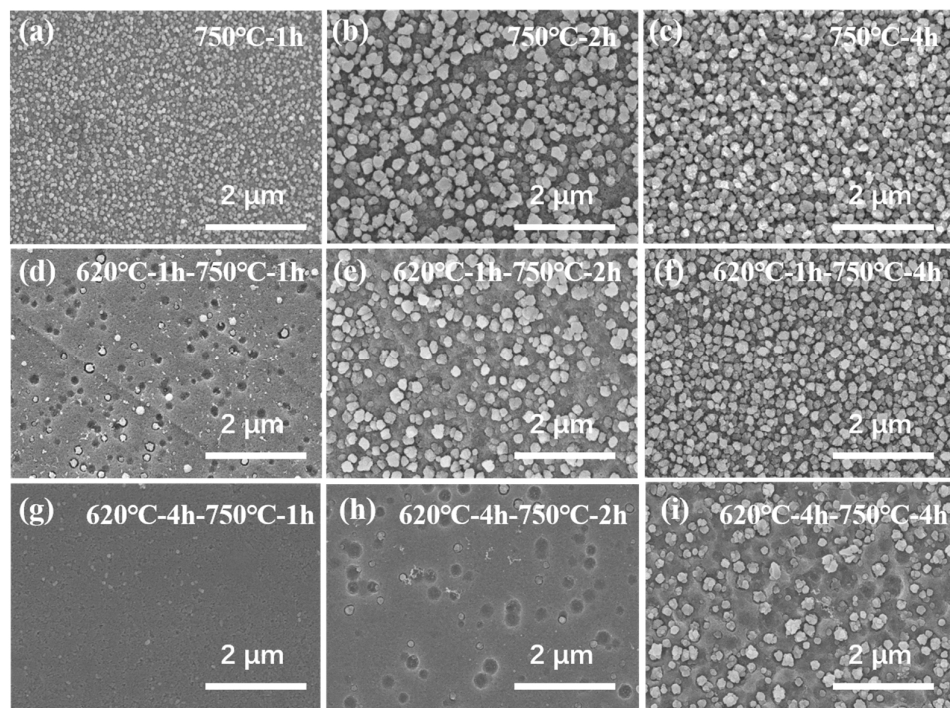


Figure 4. SEM observation on the (a) 750 °C-1 h, (b) 750 °C-2 h, (c) 750 °C-4 h, (d) 620 °C-1 h-750 °C-1 h, (e) 620 °C-1 h-750 °C-2 h, (f) 620 °C-1 h-750 °C-4 h, (g) 620 °C-4 h-750 °C-1 h, (h) 620 °C-4 h-750 °C-2 h and (i) 620 °C-4 h-750 °C-4 h.

Table 3. The crystallization fraction of different SAPLZ glass after heat treatment at 620 °C for 0 h/0.5 h /1 h/2 h/4 h and 750 °C for 1 h.

Sample	Crystallinity (%)
620 °C-0 h and 750 °C-1 h	43.7
620 °C-0.5 h and 750 °C-1 h	22.1
620 °C-1 h and 750 °C-1 h	7.2
620 °C-2 h and 750 °C-1 h	1.3
620 °C-4 h and 750 °C-1 h	0

The possible mechanism for the inhibitory effect of APS on precipitated crystal in the studied glass system is proposed, as illustrated in Figure 6. To be noted, the presence of P⁵⁺ concentration surrounding the Li-rich region can be attributed to propensity of P⁵⁺ for dissociation from the glassy network structure, which leads to the formation of isolated [PO₄] with an affinity for Li⁺ [12,19]. Subsequently, Li⁺ can effectively capture P⁵⁺ during APS, thus forming a diffusion barrier around each Li-rich droplet to inhibit further Li-related crystal growth. Meanwhile, the APS induces an increase in Q⁴ at the expense of Q³, which implies an enhanced polymerization degree in the Si-related amorphous area and subsequently increases its viscosity and raises the kinetic barrier of Si-related crystal growth.

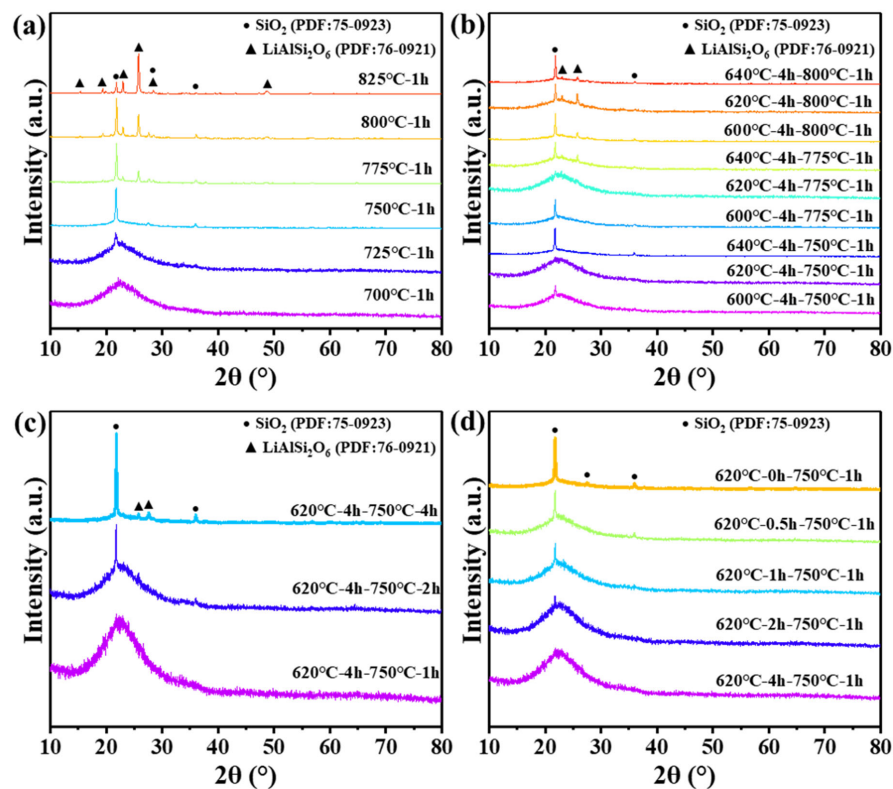


Figure 5. XRD patterns of SAPLZ glass heat-treated (a) from 700 °C to 825 °C for 1 h, (b) at 600 °C/620 °C/640 °C for 4 h and 750 °C/775 °C/800 °C for 1 h, (c) at 620 °C for 4 h and 750 °C for 1 h/2 h/4 h, and (d) at 620 °C for 0 h/0.5 h/1 h/2 h/4 h and 750 °C for 1 h.

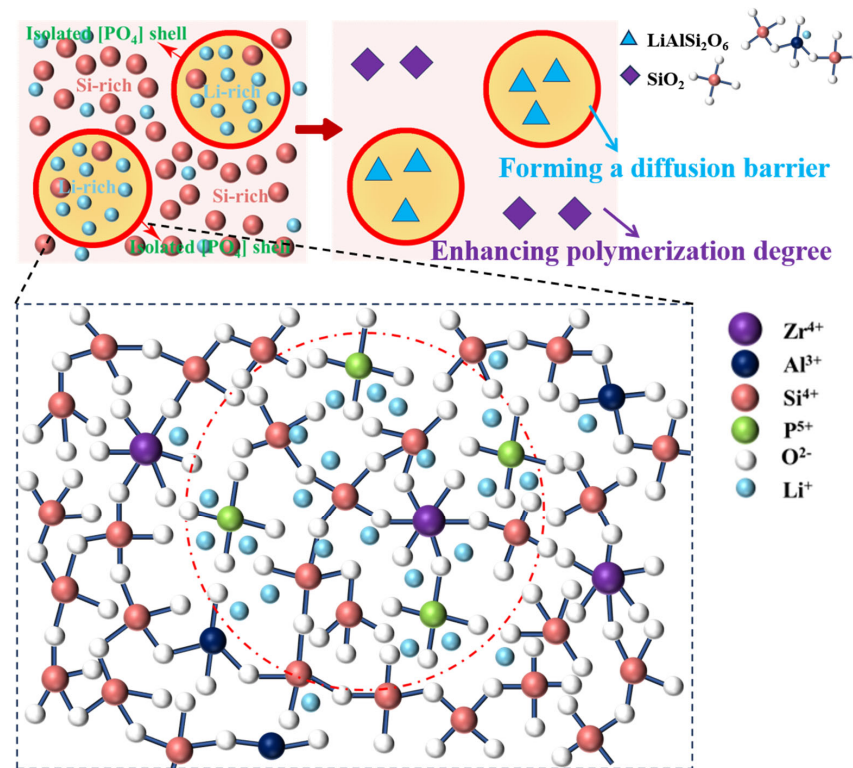


Figure 6. Schematic illustration of possible mechanism for the inhibitory effect of APS on precipitated crystal in the studied glass system.

4. Conclusions

In summary, we have proposed a new SAPLZ APS glass with robust crystallization resistance for the first time, which highlights the meticulous microstructure tunability of glass. The structure analysis shows that the APS is attributed to the Li-rich phase (surrounded by P^{5+}) and Si-rich phase. Probing into the crystallization performance of SAPLZ APS glass, anti-crystallization performance greatly improved upon introducing APS engineering, which reveals the inhibitory effect of APS on crystal growth in the studied glass system. Not only was a diffusion barrier around each Li-rich droplet formed, but the polymerization degree was increased as well in the Si-related amorphous area. This study demonstrates an effective application of APS engineering in developing new glass.

Author Contributions: M.D. contributed to conceptualization, experimental design and performance, writing, and funding acquisition; M.W. contributed to resources and project administration; Y.R. contributed to methodology and text editing; Y.X. contributed to funding acquisition, conceptualization, and supervision; D.W. contributed to investigation and data curation; S.L. contributed to funding acquisition, conceptualization, and supervision; P.L. contributed to supervision and conceptualization. All authors have read and agreed to the published version of the manuscript.

Funding: This research was supported by the National Natural Science Foundation of China (No.: U2241236, 52372014, 12304442), the Key R&D Project of Hubei Province (2022BAA025) and Natural Science Foundation of Fujian Province (2022J05091).

Data Availability Statement: Data are contained within the article.

Conflicts of Interest: Mingzhong Wang was employed by the Yichang CSG Photovoltaic Glass Co., Ltd. The remaining authors declare that the research was conducted in the absence of any commercial or financial relationships that could be construed as a potential conflict of interest. The Yichang CSG Photovoltaic Glass Co., Ltd. company was not involved in the study design, collection, analysis, interpretation of data, the writing of this article or the decision to submit it for publication.

References

1. Rawlings, R.; Wu, J.; Boccaccini, A. Glass-ceramics: Their production from wastes—A review. *J. Mater. Sci.* **2006**, *41*, 733–761. [[CrossRef](#)]
2. Zhao, M.; Cao, J.; Wang, Z.; Li, G. Insight into the dual effect of Fe_2O_3 addition on the crystallization of $CaO-MgO-Al_2O_3-SiO_2$ glass-ceramics. *J. Non-Cryst. Solids* **2019**, *513*, 144–151. [[CrossRef](#)]
3. Zheng, W.; Lin, M.; Cheng, J. Effect of phase separation on the crystallization and properties of lithium aluminosilicate glass-ceramics. *Glass Phys. Chem.* **2013**, *39*, 142–149. [[CrossRef](#)]
4. Sakamoto, A.; Himei, Y.; Hashibe, Y. β -Spodumene glass-ceramic with anomalous low thermal expansion. *Adv. Mater. Res.* **2008**, *39*, 381–386. [[CrossRef](#)]
5. Laczka, M.; Laczka, K.; Cholewa-Kowalska, K.; Kounga, A.B.; Appert, C. Mechanical properties of a lithium disilicate strengthened lithium aluminosilicate glass-ceramic. *J. Am. Ceram. Soc.* **2014**, *97*, 361–364. [[CrossRef](#)]
6. Xia, L.; Yang, Y.; Zhang, X.; Zhang, J.; Zhong, B.; Zhang, T.; Wang, H.; Wen, G. Crystal structure and wave-transparent properties of lithium aluminum silicate glass-ceramics. *Ceram. Int.* **2018**, *44*, 14896–14900. [[CrossRef](#)]
7. Rafferty, A.; Hill, R.; Wood, D. Amorphous phase separation of ionomer glasses. *J. Mater. Sci.* **2000**, *35*, 3863–3869. [[CrossRef](#)]
8. Rafferty, A.; Hill, R.; Wood, D. An investigation into the amorphous phase separation characteristics of an ionomer glass series and a sodium-boro-silicate glass system. *J. Mater. Sci.* **2003**, *38*, 2311–2319. [[CrossRef](#)]
9. Chen, Y.; Liu, S.; Zhou, Y.; Shang, P.; Shan, Z.; Zhang, J. Effect of Al_2O_3 content on amorphous phase-separation and self-limited crystallization of phosphosilicate glasses. *J. Non-Cryst. Solids* **2022**, *584*, 121505. [[CrossRef](#)]
10. Zandonà, A.; Moustros, M.; Genevois, C.; Véron, E.; Canizarès, A.; Allix, M. Glass-forming ability and ZrO_2 saturation limits in the magnesium aluminosilicate system. *Ceram. Int.* **2022**, *48*, 8433–8439. [[CrossRef](#)]
11. Lin, C.; Bocker, C.; Rüssel, C. Nanocrystallization in oxyfluoride glasses controlled by amorphous phase separation. *Nano Lett.* **2015**, *15*, 6764–6769. [[CrossRef](#)] [[PubMed](#)]
12. Liu, S.J.; Zhang, Y.F.; He, W.; Yue, Y.Z. Transparent phosphosilicate glasses containing crystals formed during cooling of melts. *J. Non-Cryst. Solids* **2011**, *357*, 3897–3900. [[CrossRef](#)]
13. Kirkpatrick, R.J.; Brow, R.K. Nuclear magnetic resonance investigation of the structures of phosphate and phosphate-containing glasses: A review. *Solid State Nucl. Magn. Reson.* **1995**, *5*, 9–21. [[CrossRef](#)] [[PubMed](#)]
14. Li, J.; Wang, M.; Lu, P. Nucleating role of P_2O_5 in nepheline-based transparent glass-ceramics. *J. Am. Ceram. Soc.* **2021**, *104*, 5614–5624. [[CrossRef](#)]

15. Zanotto, E.D.; James, P.F.; Craievich, A.F. The effects of amorphous phase separation on crystal nucleation kinetics in BaO-SiO₂ glasses. *J. Mater. Sci.* **1986**, *21*, 3050–3064. [[CrossRef](#)]
16. Zanotto, E.D. Effect of liquid phase separation on crystal nucleation in glass-formers. Case closed. *Ceram. Int.* **2020**, *46*, 24779–24791. [[CrossRef](#)]
17. CAHN, J.W. The Metastable Liquidus and Its Effect on the Crystallization of Glass. *J. Am. Ceram. Soc.* **1969**, *52*, 118–121. [[CrossRef](#)]
18. James, P.F. Glass ceramics: New compositions and uses. *J. Non-Cryst. Solids* **1995**, *181*, 1–15. [[CrossRef](#)]
19. Zhu, L.; Wang, M.; Xu, Y.; Zhang, X.; Lu, P. Dual effect of ZrO₂ on phase separation and crystallization in Li₂O-Al₂O₃-SiO₂-P₂O₅ glasses. *J. Am. Ceram. Soc.* **2022**, *105*, 5698–5710. [[CrossRef](#)]
20. Nicoleau, E.; Schuller, S.; Angeli, F.; Charpentier, T.; Jollivet, P.; Le Gac, A.; Fournier, M.; Mesbah, A.; Vasconcelos, F. Phase separation and crystallization effects on the structure and durability of molybdenum borosilicate glass. *J. Non-Cryst. Solids* **2015**, *427*, 120–133. [[CrossRef](#)]
21. James, P.F. Liquid-phase separation in glass-forming systems. *J. Mater. Sci.* **1975**, *10*, 1802–1825. [[CrossRef](#)]
22. Sycheva, G.A. Phase separation and crystallization in glasses of the lithium silicate system xLi₂O · (100 – x)SiO₂ (x = 23.4, 26.0, 33.5). *Glass Phys. Chem.* **2011**, *37*, 135–149. [[CrossRef](#)]
23. Bussey, J.M.; Weber, M.H.; Smith-Gray, N.J.; Sly, J.J.; McCloy, J.S. Examining phase separation and crystallization in glasses with X-ray nano-computed tomography. *J. Non-Cryst. Solids* **2023**, *600*, 121987. [[CrossRef](#)]
24. Zhang, L.; Eckert, H. Short-and medium-range order in sodium aluminophosphate glasses: New insights from high-resolution dipolar solid-state NMR spectroscopy. *J. Phys. Chem. B* **2006**, *110*, 8946–8958. [[CrossRef](#)] [[PubMed](#)]
25. Lang, D.P.; Alam, T.M.; Bencoe, D.N. Solid-state ³¹P/²⁷Al and ³¹P/²³Na TRAPDOR NMR investigations of the phosphorus environments in sodium aluminophosphate glasses. *Chem. Mater.* **2001**, *13*, 420–428. [[CrossRef](#)]
26. Yu, X.; Wang, M.; Rao, Y.; Xu, Y.; Xia, M.; Zhang, X.; Lu, P. Unveiling the evolution of early phase separation induced by P₂O₅ for controlling crystallization in lithium disilicate glass system. *J. Eur. Ceram. Soc.* **2023**, *43*, 5381–5389. [[CrossRef](#)]
27. Micoulaut, M. The slope equations: A universal relationship between local structure and glass transition temperature. *Eur. Phys. J. B—Condens. Matter Complex Syst.* **1998**, *1*, 277–294. [[CrossRef](#)]
28. Bradtmüller, H.; Gaddam, A.; Eckert, H.; Zanotto, E.D. Structural rearrangements during sub-T_g relaxation and nucleation in lithium disilicate glass revealed by a solid-state NMR and MD strategy. *Acta Mater.* **2022**, *240*, 118318. [[CrossRef](#)]
29. Iqbal, Y.; Lee, W.; Holland, D.; James, P. Metastable phase formation in the early stage crystallisation of lithium disilicate glass. *J. Non-Cryst. Solids* **1998**, *224*, 1–16. [[CrossRef](#)]

Disclaimer/Publisher’s Note: The statements, opinions and data contained in all publications are solely those of the individual author(s) and contributor(s) and not of MDPI and/or the editor(s). MDPI and/or the editor(s) disclaim responsibility for any injury to people or property resulting from any ideas, methods, instructions or products referred to in the content.